Reactive Collisions and Final State Analysis of C- and O-Involving Reactions Relevant to the Hypersonic Flight Regime

Meuwly, Markus
UNIVERSITAT BASEL
PETERSPLATZ 1
BASEL, BS, 4051
CHE

01/21/2022
Final Technical Report

REPORT DOCUMENTATION PAGE

PLEASE DO NOT RETURN YOUR FORM TO THE ABOVE ORGANIZATION.

1. REPORT DATE 20220121	2. REPORT TYPE Final	3. DATES COVERED	
		START DATE 20180915	END DATE 20210914

4. TITLE AND SUBTITLE
Reactive Collisions and Final State Analysis of C- and O-Involving Reactions Relevant to the Hypersonic Flight Regime

5a. CONTRACT NUMBER	5b. GRANT NUMBER FA9550-18-1-7013	5c. PROGRAM ELEMENT NUMBER 61102F
5d. PROJECT NUMBER	5e. TASK NUMBER	5f. WORK UNIT NUMBER

6. AUTHOR(S)
Markus Meuwly

7. PERFORMING ORGANIZATION NAME(S) AND ADDRESS(ES) UNIVERSITAT BASEL PETERSPLATZ 1 BASEL, BS 4051 CHE	8. PERFORMING ORGANIZATION REPORT NUMBER

9. SPONSORING/MONITORING AGENCY NAME(S) AND ADDRESS(ES) EOARD UNIT 4515 APO AE 09421-4515	10. SPONSOR/MONITOR'S ACRONYM(S) AFRL/AFOSR IOE	11. SPONSOR/MONITOR'S REPORT NUMBER(S) AFRL-AFOSR-UK-TR-2022-0017

12. DISTRIBUTION/AVAILABILITY STATEMENT
A Distribution Unlimited: PB Public Release

13. SUPPLEMENTARY NOTES

14. ABSTRACT
The determination of thermal and vibrational relaxation rates of triatomic systems suitable for application in hypersonic model calculations is discussed. For this, potential energy surfaces for ground and electronically excited state species need to be computed and represented with high accuracy and quasiclassical or quantum nuclear dynamics simulations provide the basis for determining the relevant rates. These include thermal
reaction rates, state-to-state cross sections, and vibrational relaxation rates. For exemplary systems - [NNO], [NOO], and [CNO] - all individual steps are described and a literature overview for them is provided. Finally, as some of these quantities involve considerable computational expense, for the example of state-to-state cross sections the construction of an efficient model based on neural networks is discussed. All such data is required and being used in more coarse-grained computational fluid dynamics simulations.

15. SUBJECT TERMS

16. SECURITY CLASSIFICATION OF:			17. LIMITATION OF ABSTRACT SAR	18. NUMBER OF PAGES 46
a. REPORT U	b. ABSTRACT U	c. THIS PAGE U		

19a. NAME OF RESPONSIBLE PERSON DOUGLAS SMITH	19b. PHONE NUMBER *(Include area code)* 314 235 6013

Final Report: Small-Molecule Reactions Relevant to the Hypersonic Flight Regime FA9550-18-1-7013 Reporting Period October 2018 - September 2021

Markus Meuwly*

Department of Chemistry, University of Basel, Klingelbergstrasse 80, 4056 Basel, Switzerland

E-mail: m.meuwly@unibas.ch

Abstract

The determination of thermal and vibrational relaxation rates of triatomic systems suitable for application in hypersonic model calculations is discussed. For this, potential energy surfaces for ground and electronically excited state species need to be computed and represented with high accuracy and quasiclassical or quantum nuclear dynamics simulations provide the basis for determining the relevant rates. These include thermal reaction rates, state-to-state cross sections, and vibrational relaxation rates. For exemplary systems - [NNO], [NOO], and [CNO] - all individual steps are described and a literature overview for them is provided. Finally, as some of these quantities involve considerable computational expense, for the example of state-to-state cross sections the construction of an efficient model based on neural networks is discussed. All such

1

data is required and being used in more coarse-grained computational fluid dynamics simulations.

Introduction

In hypersonic flight an object traveling at high speed through an atmosphere will dissipate large amounts of energy to the surrounding gas and generate highly non-equilibrium conditions with respect to occupation of translational, rotational, vibrational, and electronic degrees of freedom of the surrounding molecules. Typically, the energies (and hence temperatures) are sufficiently high to dissociate small molecules such as N_2 and O_2. At these extremes, the energy dissipated due to chemistry can be comparable to shock and skin friction interactions. For Earth's atmosphere the main constituents of the air at altitudes for which the medium is sufficiently dense for frequent collisions (30 km to 60 km above sea level, i.e. troposphere and stratosphere) are O_2, N_2, and NO. Mars, Titan, Venus and other planets with dense atmospheres have significantly more complex polyatomic species to consider.

Hypersonic flight is an endeavor of grand scale. A hypersonic vehicle travels at speeds of kilometers per second, experiences surface temperatures only limited by the vaporization temperature of its outer shell, is exposed to tens of MW/m^2 of heating and generates a bow shock with temperatures up to 20000 K. For example the current upper limit for velocity of a man made object is 12.5 km/s set by the Stardust capsule,[1] although natural meteors can have higher velocities ($\sim$ 70 km/s) as reported for Meteor Leonid.[2] In subsonic flight, the dynamics is driven by the flow across a surface. At supersonic speeds, the dissipation of the flow is dominated by the generation of shock waves. The characteristics of subsonic, supersonic, and hypersonic flow have been discussed at length in the literature.[3]

At hypersonic velocities, typically considered as above Mach 5,[4] the thermodynamics of the flow couples to its chemistry. In the case of Earth's atmosphere, this is primarily the dissociation of oxygen and nitrogen to atomic species which removes thermal energy but generates highly reactive species. Under such extreme flow conditions, local heating, surface ablation, control surface authority and plasma formation are directly sensitive to the energy distribution in molecules and atoms. These span a wide range of temporal (picoseconds for time vibrational relaxation; seconds for the object's travel time) and spatial (Å for molecular scales to metres for the vehicle/object) scales ($\sim 10^{12}$) between atomic and molecular collisions and macroscopic changes in the morphology or composition of matter. In other words, hypersonics is inherently a multi-scale problem.

The common approach for incorporating chemistry into CFD modeling is due to Park.[5,6] In a series of publications, the approach was developed to allow for multiple temperatures, T_v and T_t being the vibrational and translational/rotational temperatures. In application to kinetics the temperature is taken to be the geometric mean of these, the so-called "$T - T_v$ model". Additionally, following and extending the approach from Millikan and White,[7] an important intuitive correction established a framework for including the vibrational relaxation that is required for the generation of vibrational non-equilibrium.[8] With only minor variations, this approach has been applied for the last 25 years. With larger computational platforms, it has been possible to investigate the underlying physics on which the Park approach rests. For example, it was shown for N_2+N and $N_2 + N_2$ that, using the Millikan-White vibrational relaxation model, the TT_v model predicts a much faster N_2 dissociation for $T \leq 20000$ K than that obtained with direct molecular simulations whereas for $T = 30000$ K the two models agree.[9] Additional work on vibrational relaxation [10,11] shows that there is a clear difference between the modified Millikan and White model for vibrational relaxation and what is expected from high fidelity quantum mechanical or quasiclassical trajectory simulations, by up to 1 order of magnitude. Since these rates affect the major chemical species in the

flow, they will at the largest scale even influence the aerodynamic properties.

For chemical reactions most often the total collision model, based on a modified Arrhenius equation, is used,[12] although more refined models such as the general collision energy model are also available.[13] However, it would be preferable to have more detailed and accurate state-to-state models available to support hypersonic flow modeling. This is a problem as most of the cross sections presently used are derived from chemical kinetics, many of which have not historically been measured at and above 3000 K, or can not be measured but are required at even higher temperatures. However, the required information can be obtained from quasiclassical trajectory simulations using state-of-the art potential energy surfaces which will be discussed further below. Additionally, properties like vibrational relaxation times or the distribution of vibrational and rotational states often need to be inferred or modelled whereas explicit determination from rigorous atomistic simulations is likely to provide less biased quantities that can be used as input for more coarse grained modeling.

The present work summarizes the results over the past three years in terms of technical improvements and in determining essential molecular-level information for use in more coarse-grained simulations and characterization of the systems per-se, for understanding reactive and non-reactive processes at high temperatures, relevant to the hypersonic flight regime. The focus is on high-level, extensible data both, in terms of accuracy and in terms of covering chemical space. Hence, the methodological ansatz is chosen such that new reactions can be incorporated seamlessly.

Computational Methods

Molecular-level information, such as state-to-state cross sections $\sigma(\nu, j \rightarrow \nu', j'; E_\mathrm{t})$, thermal rates $k(T)$, vibrational relaxation (VR) rates, VR times, and the final state distributions of ro-vibrational states and translational energies that can be used in more coarse-grained simulations, such as DSMC, can be obtained by solving the dynamical equations for a number of selected initial conditions and computing the relevant observables. This is not only useful for coarse grained models but also a very valuable source for comparison and interpretation of laboratory-based experiments. Solving the dynamical equations can be done either by adopting a quantum mechanical (QM) or a classical mechanical viewpoint. When using a QM-based method, a time-independent or time-dependent formalism has to be employed. For classical simulations the most common approach uses quasi-classical trajectory (QCT) studies. For both such studies the intermolecular potential energy surface (PES) encapsulates the totality of physical interactions for a given electronic state for all atoms involved and provides the most fundamental level to address the problem at hand. These points are discussed in some more detail in the next few sections within the limit that the electronic states are considered separate entities and that the electrons can move significantly faster than the nuclei (Born-Oppenheimer approximation).

Electronic Structure Calculations

Exploring the electronic structures for different critical configurations (i.e., stationary points and entrance or exit channels) is the first and foremost part prior to constructing a full-dimensional PES. This gives an impression about the number of electronic states important in studying the collision dynamics of a particular system and also provides knowledge about the nature of the electronic wavefunctions at the critical regions. The C-, N-, and O-containing species show highly multireference character near the asymptotic regions and

single reference methods typically fail to describe those regions of the PES. Hence, a multi reference configurations interaction (MRCI) method is necessary to provide an accurate description of the energetics, in particular for electronically excited states.

Complete active space self-consistent field (CASSCF)[14–16] calculations are performed prior to MRCI calculations to generate the initial wave function. However, single state CASSCF method often fails to converge near the avoided crossing regions and state averaged (SA) CASSCF calculations are therefore prescribed. All the important electronic states with different possible spin and spatial symmetries are included in the SA-CASSCF calculations. MRCI calculations are then performed for a particular state starting from the SA-CASSCF wavefunction with equal weight on each of the electronic states. Dynamically weighted SA-CASSCF calculations are also performed in some cases. Davidson corrections (MRCI+Q)[17–19] are used to reduce the size consistency error. Basis functions are chosen to provide a healthy balance between accuracy and computational expense. The augmented Dunning-type correlation consistent polarize triple zeta (aug-cc-pVTZ)[20] are generally enough to give proper description of the systems. Explicitly correlated MRCI (MRCI-F12) methods can also be used to reduce errors originating from the finite size of the atomic basis set.

Non-reactive and Reactive Potential Energy Surfaces

Due to continuous improvements of computer architectures and efficiency gains in the numerical methods, fully-dimensional PESs for triatomic systems can now be routinely calculated at the coupled-cluster or multi-reference configuration interaction (MRCI) level of theory. For smaller electronic systems even full CI (FCI) treatments with large basis sets are possible.[21] A complete coverage for a triatomic, reactive systems (A+BC→AB+C) requires of the order of 10^4 energy evaluations. Hence, over the past few years the challenge has partially

shifted away from the computation of reference energies to representing them.

For dynamics calculations continuous PESs covering all energies accessed by the simulations are required. Possibilities to *represent* the *ab initio* calculated energies include conventional parametrized fits, the modified Shepard interpolation,[22–24] the moving least squares method,[25–27] permutation invariant polynomials[28–30] or neural network approaches[31–33] to obtain multi-dimensional reactive PESs.[34–40] Another approach is based on reproducing kernel Hilbert spaces (RKHS) which attempts to *exactly represent* the energies instead of finding an acceptable approximation to them.[41–44]

Machine-learning (ML) methods provide estimates for a function value given input $\mathbf{x}$ (e.g. all Cartesian coordinates of a system) using a model that was "trained" on a set of known data.[45] For intermolecular interactions, the use of reproducing kernel Hilbert space (RKHS) theory[46] provides means to construct a PES from a training set based on *ab initio* reference data.[41–43] Such an approach is typically referred to as kernel ridge regression (KRR).[45,47] The RKHS method has been successfully applied e.g. for constructing PESs for CNO,[48] N_2^+–Ar[49] or H_2O.[50] A combination of expanding the PES in spherical harmonics for the angular coordinates and reproducing kernels for the radial coordinates has been explored for H_2^+–He[51] and is now also used for larger systems.[52,53]

To further automatize this process, dedicated computer code has been made available that generates the interpolation (and meaningful extrapolation) of the PES along with all required parameters automatically from girded *ab initio* data.[44] The theory of reproducing kernel Hilbert spaces asserts that for given values $f_i = f(\mathbf{x}_i)$ of a function $f(\mathbf{x})$ for N training points $\mathbf{x}_i$, $f(\mathbf{x})$ can always be approximated as a linear combination of kernel products[54]

$$\widetilde{f}(\mathbf{x}) = \sum_{i=1}^{N} c_i K(\mathbf{x}, \mathbf{x}_i) \tag{1}$$

7

Here, the c_i are coefficients and $K(\mathbf{x}, \mathbf{x}')$ is the reproducing kernel of the RKHS. The coefficients c_i satisfy the linear relation

$$f_j = \sum_{i=1}^{N} c_i K_{ij} \tag{2}$$

with the symmetric, positive-definite kernel matrix $K_{ij} = K(\mathbf{x}_i, \mathbf{x}_j)$ and can therefore be calculated from the known values f_i in the training set by solving Eq. 2 for the unknowns c_i using, e.g. Cholesky decomposition.[55] With the coefficients c_i determined, the function value at an arbitrary position $\mathbf{x}$ can be calculated using Eq. 1. Derivatives of $\widetilde{f}(\mathbf{x})$ of any order can be calculated analytically by replacing the kernel function $K(\mathbf{x}, \mathbf{x}')$ in Eq. 1 with its corresponding derivative.

The explicit form of the multi-dimensional kernel function $K(\mathbf{x}, \mathbf{x}')$ is chosen depending on the problem to be solved. In general, it is possible to construct D-dimensional kernels as tensor products of one-dimensional kernels $k(x, x')$

$$K(\mathbf{x}, \mathbf{x}') = \prod_{d=1}^{D} k^{(d)}(x^{(d)}, x'^{(d)}) \tag{3}$$

For the kernel functions $k(x, x')$ it is possible to encode physical knowledge, in particular about their long range behaviour. Explicit radial kernels include the reciprocal power decay kernel[41]

$$k_{n,m}(x, x') = n^2 x_>^{-(m+1)} B(m+1, n)_2 F_1\left(-n+1, m+1; n+m+1; \frac{x_<}{x_>}\right) \tag{4}$$

or the exponential decay kernel

$$k_n(x, x') = \frac{n \cdot n!}{\beta^{2n-1}} e^{-\beta x_>} \sum_{k=0}^{n-1} \frac{(2n-2-k)!}{(n-1-k)!k!} [\beta(x_> - x_<)]^k \tag{5}$$

where $x_>$ and $x_<$ are the larger and smaller of x and x' and the integer n determines the

smoothness. In Eq. 4 the parameter m is the long-range decay of the dominant intermolecular interaction (e.g. $m = 5$ for dispersion), $B(a, b)$ is the beta function and $_2F_1(a, b; c; d)$ is the Gauss hypergeometric function.

One particular challenge in extending these methods to larger systems (tetra- or penta-atomic systems) is therefore to reduce the number of reference energies while maintaining an accurate representation of the global PES. Considerable progress in this regard has been recently made by using either Gaussian Processes combined with Bayesian inference[56] or by optimizing permutationally invariant polynomials (PIPs).[57]

An alternative approach uses the known long-range form of the interaction potential, a model (e.g. a Morse curve) for the short range together the statistical adiabatic channel model to determine capture rates.[58,59] Such an approach is reminiscent of using empirical forms of the potential energy surfaces for studying the high resolution spectroscopy of van der Waals complexes.[60] One of the advantages over more recent fitting approaches of reference electronic structure data is the possibility to examine the role of specific features of the PES on the observables. As an example, the influence of potential anisotropy on the reaction rate[58] or vibrational relaxation can be examined in a controlled fashion. On the other hand, such an approach does not necessarily yield a globally valid PES and depends on the quality of the experimental data.

For non-reactive collisions (e.g., $Ar+CO$[11]), PESs are computed only for the reactant channel. However, in order to allow chemical reactions to be described, bonds need to be broken and formed. A full-dimensional PES describing all the asymptotes/channels are thus necessary. This is done by mixing the PESs[61] of all possible channels of reactants and products using smooth switching functions, parametrized in a fashion as to best capture the potential well and the barrier crossing regions.

Nuclear Dynamics

With global PESs in place, it is then possible to determine state-to-state cross sections and rates from which total cross sections and thermal rates can be computed. This information together with the vibrational relaxation times are the main ingredients for the CFD and DSMC simulations mentioned in the Introduction. These quantities can be determined either from quasiclassical trajectory (QCT) simulations or from numerical solutions of the nuclear Schrödinger equation. For both approaches suitable reviews exist.[62–64]

Quasiclassical Trajectories: In QCT simulations, Newton's (or Hamilton's) equations of motion are propagated using a numerical integration in time. The dynamics is governed by the multidimensional PESs and the initial conditions for $\mathbf{x}$ and $\mathbf{v}$ (or $\mathbf{p}$ and $\mathbf{q}$) are generated according to a Monte Carlo scheme. Typical propagators are the velocity verlet integrator or Runge-Kutta of different orders. The reactant and product ro-vibrational states are determined following semiclassical quantization. Since the ro-vibrational states of the product diatom are continuous numbers, the states are assigned by rounding to integer values either from histogram binning (rounding to the nearest integer) or Gaussian binning which weights each trajectory with a Gaussian shaped function centered on the integer values.[65–67]

The state-to-state reaction cross section at fixed collision energy E_c is $\sigma_{v,j \to v',j'}(E_c) = 2\pi \int_0^{b_{\max}} P_{v,j \to v',j'}(b; E_c) b db$. Monte Carlo sampling of this integral yields[62]

$$\sigma_{v,j \to v',j'}(E_c) = \pi b_{\max}^2 \frac{N_{v',j'}}{N_{\text{tot}}}, \tag{6}$$

where N_{tot} is the total number of trajectories, $N_{v',j'}$ is the number of reactive trajectories for final state (v', j'), and $b_{\max}$ is the maximum impact parameter for which a reactive collision

occurs. The thermal rate for temperature T is obtained from

$$k(T) = g(T)\sqrt{\frac{8k_{\mathrm{B}}T}{\pi\mu}}\pi b_{\max}^2 \frac{N_r}{N_{\mathrm{tot}}}, \tag{7}$$

where $g(T)$ is the electronic degeneracy factor, μ is the reduced mass of the collision system, k_{B} is the Boltzmann constant, and, depending on the specific process considered, N_r is the number of reactive or vibrationally relaxed trajectories. In the rate coefficient calculations, the initial ro-vibrational states and relative translational energy (E_{c}) of the reactants for the trajectories are sampled from Boltzmann and Maxwell-Boltzmann distribution at a given T, respectively. Such a treatment neglects the wave nature of the propagation so it is necessary to validate under what conditions quantum effects are expected to be significant.

Nonadiabatic Effects: Because at hypersonic conditions the energetically accessible PESs may cross, it is also relevant to consider nonadiabatic effects. For describing such transitions several trajectory-based methods exist. They include, for example,[68] fewest switches surface hopping (FSSH),[69] the Ehrenfest mean field approach,[70] or trajectory surface hopping (TSH)[71] within the Landau-Zener (LZ)[72,73] formalism. For the LZ approach the transition probability $P_{\mathrm{LZ}}^{i\to j}$ from state j to k is[48,74,75]

$$P_{\mathrm{LZ}}^{i\to j} = \exp\left(-\frac{\pi}{2\hbar}\sqrt{\frac{\Delta V_{ij}^a(R(t_c))^3}{\frac{d^2}{dt^2}\Delta V_{ij}^a(R(t_c))}}\right). \tag{8}$$

where $\Delta V_{ij}^a(R(t_c))$ is the adiabatic energy difference between states i and j at configuration R and time t_c. In practice, trajectories are started from a given initial electronic state i. If there is a crossing between the present electronic state i and a different state $j \neq i$, $P_{\mathrm{LZ}}^{i\to j}$ is calculated and compared with a random number $\xi \in [0,1]$. For $P_{\mathrm{LZ}}^{i\to j} \geq \xi$ the trajectory hops from state i to state j. To ensure conservation of total energy and total angular momentum,

11

momentum corrections along different degrees of freedom have been employed[76]

$$\mathbf{p}' = \mathbf{p} - \hat{\mathbf{n}}\frac{\hat{\mathbf{n}}\mathbf{M}^{-1}\mathbf{p}}{\hat{\mathbf{n}}\mathbf{M}^{-1}\hat{\mathbf{n}}}\left[1 - \left(1 - 2\Delta\mathrm{E}\frac{\hat{\mathbf{n}}\mathbf{M}^{-1}\hat{\mathbf{n}}}{(\hat{\mathbf{n}}\mathbf{M}^{-1}\mathbf{p})^2}\right)^{1/2}\right], \tag{9}$$

where $\mathbf{p}$ and $\mathbf{p}'$ are the momenta before and after the hop and M is the mass matrix.

Quantum Dynamics: In the high-temperature limit classical MD simulations are expected to provide a realistic description for the dynamics. However, as T decreases, nuclear effects (including zero point motion, coherence or tunneling) may become more important. The nuclear Schrödinger equation can either be solved within a time-dependent (TD) or a time-independent (TI) formalism.[64,77] For the current problem of determining state-to-state cross sections, quantum reactive scattering calculations need to be carried out. For reactive and non-reactive TI scattering calculations, general programs have been made available, including MOLSCAT,[78] Dynasol[79] or ABC.[80] In all cases the state-to-state reaction probabilities are calculated for a partial wave (J) and a particular collision energy E_c from the scattering matrix. The state-to-state cross sections $\sigma_{v'j'\leftarrow vj}(E_c)$ are then calculated by summing the probabilities of all partial waves. In each run probabilities can be calculated for only one E_c. Calculating the state-to-state cross sections as a function of E_c is thus computationally prohibitive. However, as the time is not directly involved in the calculations, observables can be calculated down to very low collision energies.

Alternatively, in a time-dependent quantum mechanical (TDQM) approach[63,81,82] an initial wavefunction is written as superposition of wavefunctions (i.e., wave packet) and the wave packet (WP) is propagated in time and finally, the flux is calculated at the product/reactant channels to determine the reaction probabilities. The most widely used representation is based on Gaussian coherent states which cover a range of energies. To evaluate the action of the Hamiltonian on the WP it is advantageous to either work in momentum space and use

Fast Fourier transform techniques or to use the coordinate representation together with a discrete variable representation (DVR). For propagating the WP in time the split-operator,[83] Chebyshev[84–88] or iterative Lanczos techniques can be used. As a spatially finite grid is used to represent the WP, reflection from the grid boundary need to be suppressed by using either complex absorbing potentials or damping functions at the grid boundary.[89,90] With these elements in place, the initial WP can be propagated in time and space until a given final time for which the WP can be projected onto a final state. Because the WP contains a continuum of collision energies extending over a finite range, in each run probabilities can be calculated for a range of energies depending on the WP for a particular initial state. One of the limitations of a TD approach is for systems with deep bound wells which require long propagation times until final states are reached. Similarly, computing reaction attributes at very low collision energies are challenging due to long time propagation.

Quantum dynamical calculations for C-, N-, and O-containing triatomics have mainly been carried out to determine reaction probabilities and cross sections at given collision energies.[91–95] However, to calculate the rates, cross sections are summed over a range of E_c for a given temperature and a large number of partial waves are needed to converge the cross sections for high collision energies. Hence, the J-interpolated probabilities are used to calculate the cross sections and rates thereafter.[93,96] At high temperatures more ro-vibrational states are populated and the translational energy range to cover also increases which adds a large number of separate calculations for each rotational state (j), its $k-$component (projection of j on z-axis) and partial waves (J) to obtain converged results. Hence, the computation of reaction cross sections becomes prohibitive and simulations for hypersonic flow based on data from quantum dynamics simulations thus is probably intractable. Even with these limits, quantum dynamics simulations provide a means of accessing the appropriateness of computationally cheaper QCT approaches and their implicit simplifying approximations.

Results and Discussion

State-to-State, Thermal Rates and Vibrational Relaxation Rates

As already indicated in the Introduction, hypersonics requires thermal and state-to-state nonreactive and reactive cross sections and vibrational relaxation times. These ingredients are then used in more coarse-grained simulations of the state distribution of the species involved to characterize the nonequilibrium chemistry around an object traveling at high speed through a gaseous atmosphere.

In the following, previous and more recent efforts to determine such quantities from atomistic simulations and quantum treatments of the nuclear dynamics are described, in particular for the [NOO], [NNO], [CNO] systems. A set of particularly relevant reactions, the Zeldovich or "thermal NO mechanism",[97] includes the (NO + O / O$_2$ + N) and (NO + N / N$_2$ + O) reactions[98,99] that describe the oxidation of nitrogen. These reactions, together with a range of other atom plus diatom and diatom plus diatom reactions form the core of the 5- and 11-species model used in hypersonics.[100]

At high temperatures ($\sim$ 20000 K), as present in thin regions of shock layers created at hypersonic speed flight,[5] the reactive chemical processes can become very complex. Part of the complexity arises due to higher electronically excited states that become accessible, and another part is due to thermal non-equilibrium. When higher electronically excited states need to be included, 3-dimensional PESs for them need to be calculated, too, and nonadiabatic transitions between them may become possible.

The [NOO] System: The N(^{4}S) + O$_2$(X$^3\Sigma_g^-$) $\leftrightarrow$ O(^{3}P) + NO(X$^2\Pi$) reaction is one of the N- and O- involving reactions relevant to the reactive air flow around spacecraft during hypersonic atmospheric reentry. Furthermore, the NO-involving reactions connect the dom-

inating species N_2 and O_2. To study the dynamics of the forward and backward reactions, PESs for $^2A'$, $^2A''$ and $^4A'$ electronic states are necessary. To compute the thermal reaction rates for the forward and the reverse reactions, equilibrium constants, PESs for $^2A'$ and $^4A'$ electronic states of NO_2 are needed. However, the $^4A'$ state has a barrier of $\sim$1.6 eV for the O+NO collisions and this state contributes less to the vibrational relaxation. The $^2A''$ state has a deep potential well of $\sim$1.6 eV in the O+NO channel which leads to efficient vibrational relaxation via complex formation. PESs for those three electronic states have been calculated at different level of theory in different works by various groups.[101–105]

Thermal rates have been determined for the forward reaction at many instances using experiments and computations.[101,105–111] However, for the reverse reaction, theoretical rates[101] are determined indirectly from the equilibrium constant of $N(^4S) + O_2(X^3\Sigma_g^-) \leftrightarrow O(^3P) + NO(X^2\Pi)$. In Ref.,[105] explicit QCT calculations were carried out to calculate the rates for forward and reverse reactions for a wide range of temperatures which are in good agreement with the experiment results (see Figure 1). The equilibrium constants were also calculated for this reactive system and found to be in good agreement with the CEA[112] data base. Parameters corresponds to a modified Arrhenius equation are provided for the forward and reverse reaction rates.

Figure 2 shows the vibrational relaxation rates for the O+NO collisions for $v = 1 \rightarrow v' = 0$. Both the nonreactive and the oxygen exchange collisions contribute to the vibrational relaxation. Recent QCT simulations[116] based on the DIM PES for the $^2A'$ state[102] and a fitted DMBE PES based on 1681 MRCI/AVQZ calculations for the $^2A''$ state[103] report a value of $k_{\nu=1\rightarrow0}(T = 298K) = 4.34 \pm 0.7(10^{-11})$ cm^{3}s^{-1}. Another computational study,[115] using a 3-dimensional spline representation of energies from CASSCF/aug-cc-pVTZ calculations, reported a value of $k_{\nu=1\rightarrow0}(T = 300K) \sim 5(10^{-11})$ cm^{3}s^{-1}. These relaxation rates agree quite favourably with experiment[113,119] but the $T-$dependence of the simulations using the

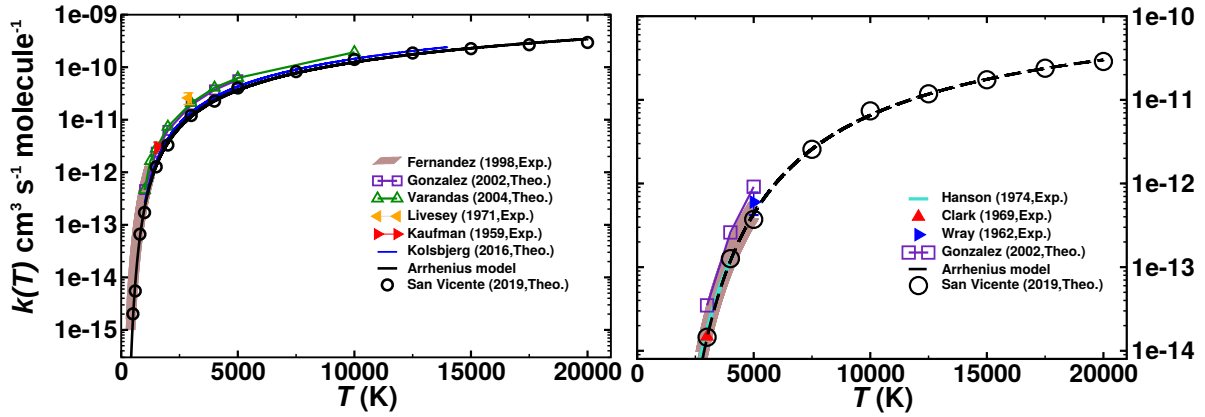Figure 1: Total rates for the $N(^4S) + O_2(X^3\Sigma_g^-) \leftrightarrow O(^3P) + NO(X^2\Pi)$ reactions. The left panel shows the rates for the forward reaction and the right panel show the rates for the reverse reaction. Arrhenius model are fits of the rates from Ref.[105] to a modified Arrhenius model. Data taken from Ref.[105]
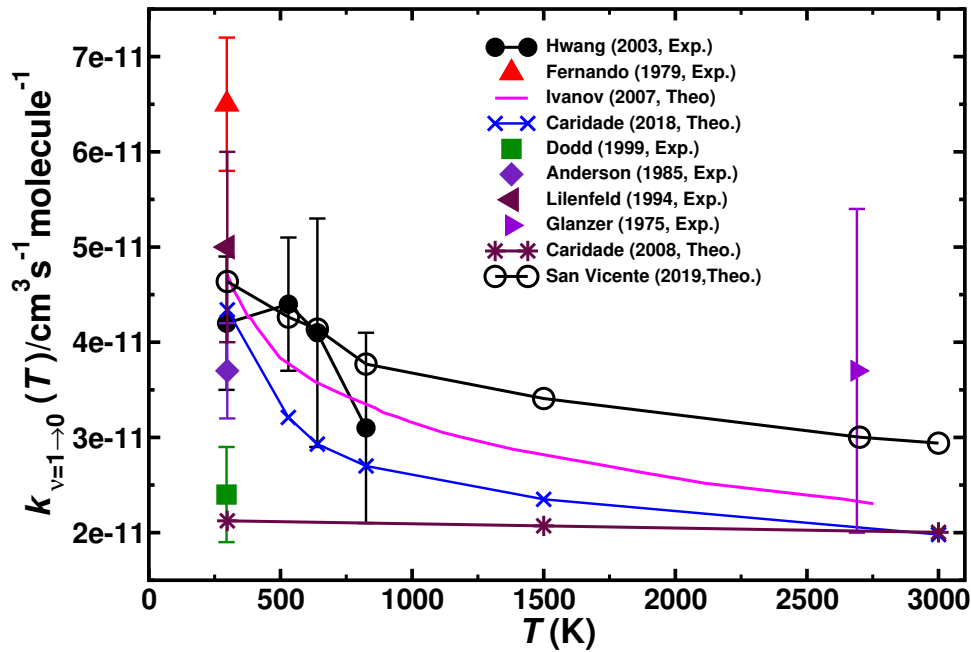

Figure 2: Vibrational relaxation rates for $O+NO(\nu = 1) \rightarrow O+NO(\nu' = 0)$. Symbols with error bars show the experimentally determined VR rates and Symbols connected by lines show the QCT VR rates.[99,105,113–120] Data taken from Ref.[105]

16

DMBE PESs is too steep, in particular for the $^2A''$ state which leads to an underestimation of the vibrational relaxation at higher temperatures. More recent simulations based on RKHS-represented PESs at the MRCI/aug-cc-pVTZ level of theory correctly describe both, the low- and high-T vibrational relaxation rates as observed experimentally.[105]

The [NNO] System: The NO + N $\leftrightarrow$ O + N$_2$ reactions are important in high temperature gas flows. These reactions control the concentration of NO in the hypersonic flow during reentry. The two lowest triplet PESs ($^3A'$ and $^3A''$) of N$_2$O correlate with NO(X$^2\Pi$)+N(^4S) and N$_2$(X$^1\Sigma_g^+$)+O(^3P). In the absence of spin-orbit coupling, the NO(X$^2\Pi$)+N(^4S) $\leftrightarrow$ O(^3P) + N$_2$(X$^1\Sigma_g^+$) reactions occur entirely in the triplet manifold of N$_2$O. Several *ab initio* energy based PESs have been constructed to study the reaction dynamics of this system by fitting to polynomial functions[121,122] or representing by reproducing kernel.[123]

Rate coefficients for the forward and the reverse reactions have been estimated via experiments using different techniques. In a discharge flow-resonance fluorescence (DF-RF) and flash photolysis-resonance fluorescence the rate for the forward reaction was measured to be $3.4\pm0.9\times10^{-11}$cm^{3}s^{-1}molecule^{-1} over the temperature range 196–400 K.[124] In two different shock tube studies,[125,126] the rates were estimated over temperature ranges 1850–3160 K and 1251–3152 K as 3.32×10^{-11} and 3.7×10^{-11} cm^{3}s^{-1}molecule^{-1}, respectively. In a continuous supersonic flow reactor[127] the rates for the forward reaction were measured at 48–211 K to be $(3.2\pm0.6)\times10^{-11}\exp(25\pm16/T)$cm^{3}s^{-1}molecule^{-1}. For the reverse reaction, in shock tube experiment, the rates were expressed as $3.055\times10^{-10}\exp(38370/T)$ at 2384–3850 K temperatures.[128] In another shock tube experiment[129] the rates for the reverse reaction were measured at 2400–4100 K to be $3.0\times10^{-10}\exp(-38300/T)\pm40\%$ cm^{3}s^{-1}molecule^{-1}.

Rate coefficients for the forward and the reverse reactions have been calculated from QCT and quantum simulations for temperatures $100 \leq T \leq 5000$ K.[94,121,123,130,131] Computed rates

for both reactions are shown along with the experimental rates and Baulch recommended values[108,124–128,132–134] in Figure 3. For the forward reaction, except the ICVT/CCI rates from Ref.[121] and QCT rates from Ref.,[123] good agreement between theory and experiment is found. At high temperatures rates obtained from all the simulations are close to each other. The calculations suggest that up to ~ 5000 K N_2 formation occurs mostly on the $^3A''$ PES whereas reactions involving the $^3A'$ state start to contribute at higher temperatures. High temperature rates up to 20000 K and final state distributions for the forward reaction have been reported in Ref.[123] The reverse reaction and the N_2 dissociation are also studied recently and rate expressions are reported.[135,136] In another recent study the PESs for the two lowest triplet states of N_2O have been reconsidered based on MRCI+Q/aug-cc-pVTZ calculations.[137] The grid was considerably extended, in particular for the diatomic separation (r), and in the long range interaction region (along R) was treated more accurately. For both reactions, thermal rates are calculated on the new PESs, which are in good agreement with experiment, see open black circles in Figure 3. Upon inspection, the difference between the previous[123] and the improved, more recent PESs[137] is the presence of a small barrier in the N+NO entrance channel for the $^3A''$ state in the former which which leads to a smaller rates at low temperatures. However, the new PESs[137] show the correct behaviour of $k(T)$ at low temperatures.

For vibrational relaxation $N_2(v = 1, j) + O \rightarrow N_2(v' = 0, j) + O$ the rates from the experimental data[138–140] are extracted from the vibrational relaxation time parameters $(p\tau_{\mathrm{vib}})$ following the Bethe-Teller model.[141] In a recent study,[136] QCT calculated VR rates are found to significantly underestimate the experimental results. The VR rates calculated from QCT simulations in this work using the HB and GB schemes are shown in Figure 4. It can be seen in Figure 4 that the QCT-GB results are in a fair agreement with the experiment. However, it is noticed that if the trajectories with $\varepsilon_{0,j'} \leq \varepsilon_{v',j'} \leq \varepsilon_{0,j'} + 0.075$ eV (0.075 eV ≈ 0.3 quanta) are considered as VR trajectories, the results agree well with experiment (see Figure
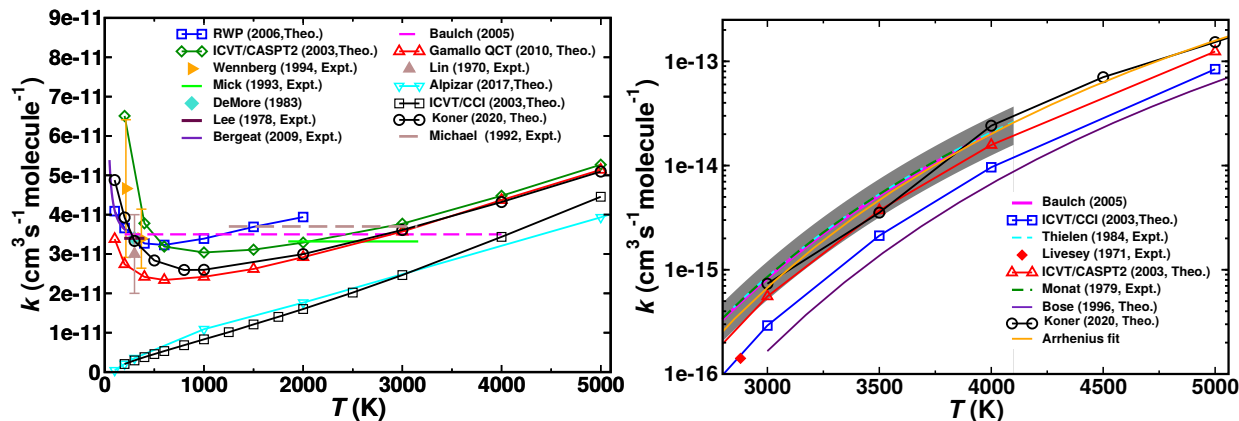
Figure 3: Rate coefficients for the NO(X$^2\Pi$)+N(^4S) $\leftrightarrow$ N$_2$(X$^1\Sigma_g^+$)+O(^3P) as a function of temperature. Left panel shows rates for the forward reaction while the right panel shows the rates for the backward reaction. The results calculated in the present work are shown as lines with open circles. Experimental (assigned as 'Expt.') and Theoretical rates (assigned as 'Theo.') available in the literature are shown.[94,108,121,123–128,130–134] Data taken from Ref.[137]

4, green line with asterisk QCT-MHB). Hence it is possible that a fraction of the trajectories which do not enter or remain in the strong coupling region for shorter time exchange only small amounts of energy and are not fully relaxed. However, to further clarify whether this is due to shortcomings in the binning strategy, sensitivity analyses of the quality of the PESs and quantum simulations are required.

The [CNO] System: Three reactive processes can be considered for this system: (i) C+NO, (ii) O+CN and (iii) N+CO. The electronic states, important to study the dynamics of (i)–(iii) collisions are ^{2}A′, ^{2}A″ and ^{4}A″. The ^{2}A′ and ^{2}A″ states connect the C(^{3}P)+NO(X$^2\Pi$), O(^{3}P)+CN(X$^2\Sigma^+$) and N(^{2}D)+CO(X$^1\Sigma^+$) channels while the ^{4}A″ state connects the C(^{3}P)+NO(X$^2\Pi$), O(^{3}P)+CN(X$^2\Sigma^+$) and N(^{4}S)+CO(X$^1\Sigma^+$) channels. The C+NO → O+CN, N+CO reactions play crucial role in removing NO from the atmosphere ("NO reburning")[143] and the CN+O and CO+N reactions are important for combustion in flames and for entry into the atmospheres of Mars or Venus.[144]

Thermal rates for the C(^{3}P)/C(^{1}D) + NO → O + CN were measured experimentally to be

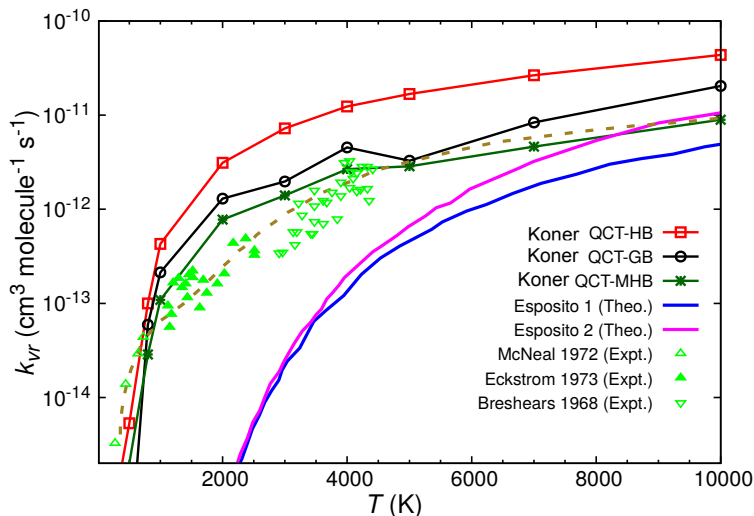Figure 4: Vibrational relaxation rates for $O+N_2(\nu = 1) \to O+N_2(\nu' = 0)$. Green symbols represent the experimentally determined VR rates.[138–140] Olive dashed line is a double Arrhenius type fit to the experimental result.[142] Rates obtained in this work from QCT simulations and using HB and GB schemes are given along with the full QCT (magenta solid line) and quasi-reactive QCT (blue solid line) results from Ref.[136] Data taken from Ref.[137]

$7.3 \pm 2.2 \times 10^{-11}$ cm^3 molecule^{-1} s^{-1} in the gas phase at room temperature[145] and later recalculated as $4.8 \pm 0.8 \times 10^{-11}$ cm^3 molecule^{-1} s^{-1}.[146] In a shock tube experiment, the rates and branching ratios of products were measured for the C+NO reaction over temperature range of 1550 – 4050 K.[147] and found to be constant. Rate coefficients for the same reaction were found to decrease with increasing temperature.[148] Analytical PESs have been constructed form CASPT2 energies for the calculations and the same parametrization of the PES were constructed for the $^2A'$, $^2A''$ and $^4A''$ electronic states of CNO[149–152] and subsequent dynamics by means of QCT[150–153] and adiabatic capture calculations[154] result thermal rates close to the experimental ones but the branching ratios of CO and CN products underestimate the experimental values. A more accurate DMBE PES for the $^2A'$ electronic state of [CNO] has been computed at MRCI-F12/cc-pVQZ-F12 level of theories and quasiclassical dynamics have been carried out but not compared with the experiment because a single PES is not sufficient to describe the dynamics.[155,156]

In recent work,[48] $\sim$ 50000 MRCI+Q/aug-cc-pVTZ energies have been used to construct

20

accurate RKHS-based representations of the 3 global PESs for the $^2A'$, $^2A''$ and $^4A''$ states of [CNO] with root mean squared errors of 0.38, 0.48 and 0.47 kcal/mol, respectively. Subsequent quasiclassical dynamics study on those RKHS PESs within recent formulations of the Landau-Zener[72,73,75,157] formalism yield thermal rates which agree well with experiment for temperatures between 50 K and 5000 K. Including nonadiabatic transitions improve the branching ratios to be compared with the experimental findings. The vibrational relaxation rates for $C(^3P) + NO(X^2\Pi)(v = 1, j) \rightarrow C(^3P) + NO(X^2\Pi)(v' = 0, j)$ are also calculated. Explicit fit to Arrhenius equation are provided for the C+NO reaction up to 20000 K.

Table 1: Parameters obtained from fitting the rates for different reactions to a modified Arrhenius equation ($k(T) = AT^n\exp(-E_a/T)$). Rate coefficients computed using these parameters have units in cm^{3}molecule^{-1}s^{-1} with $[A] = $ cm^{3}molecule^{-1}s^{-1} and $[E_a] = $ K while n is unitless.

Reaction	T(K)	A	n	E_a
$O(^3P)+NO(X^2\Pi)\rightarrow N(^4S)+O_2(X^3\Sigma_g^-)$	3000–20000	7.95872×10^{-13}	0.48656	23749.0
$N(^4S)+O_2(X^3\Sigma_g^-)\rightarrow O(^3P)+NO(X^2\Pi)$	500–20000	3.70470×10^{-15}	1.17593	4090.1
$N(^4S)+NO(X^2\Pi)\rightarrow O(^3P)+N_2(X^1\Sigma_g^+)$	2000–18000	2.17214×10^{-14}	0.88796	-946.0
$O(^3P)+N_2(X^1\Sigma_g^+)\rightarrow N(^4S)+NO(X^2\Pi)$	3000–20000	7.73865×10^{-12}	0.46177	39123.1
$O(^3P)+N_2(X^1\Sigma_g^+)\rightarrow 2N(^4S)+O(^3P)$	8000–20000	4.55027	−2.00227	129692.6
$C(^3P)+NO(X^2\Pi)\rightarrow O(^3P)+CN(X^2\Sigma^+)$	5000–20000	2.96396×10^{-13}	0.55000	-1043.3
$C(^3P)+NO(X^2\Pi)\rightarrow N(^2D)+CO(X^1\Sigma^+)$	2000–20000	3.76536×10^{-13}	0.49438	-729.1
$C(^3P)+NO(X^2\Pi)\rightarrow N(^4S)+CO(X^1\Sigma^+)$	700–18000	5.93636×10^{-15}	0.94205	-607.7

Table 1 summarizes the parameters from a modified Arrhenius equation $k(T) = AT^n\exp(-E_a/T)$ which was fitted to the rates for different reactions containing C-, N-, and O-species. The rates were computed from extensive QCT calculations on accurate RKHS PESs based on MRCI+Q/aug-cc-pVTZ ab $initio$ energies.[48,105,137] For all the reactions the rates are in good agreement with available experimental results (see Figures 1, 3) over the temperature range $\sim 50 - 5000$ K and allow predictions at considerably higher (~ 20000 K). Such expressions for the thermal rates are particularly relevant in more coarse grained simulations such as DSMC.[158]

Machine Learning Final States

Up to this point the necessary microscopic dynamics from which cross sections, thermal and vibrational relaxation rates was determined "on demand" from a given set of initial states by running explicit QCT simulations. However, such an approach can be computationally prohibitive in multi scale particle simulations, such as DSMC which attempt to solve a spatio-temporal thermochemical model by decomposing space around an object into cells the size of which is given by the local mean-free-path, i.e small close to the vehicle and large further away from it. In each of the cells chemical processes can occur and the necessary information for modeling the temporal and spatial evolution needs to be determined from either explicit QCT simulations or from evaluating a simplified model.

As the number of particles ranges from 10^5 to 10^{10} and the simulation time scales are macroscopic, efficient cross section models are required.[158] For a diatomic molecule there are on the order of $\sim 10^4$ internal (v, j) states. For atom+diatom collision this leads to $\sim 10^8$ state-to-state transitions for which on the order of 10^{15} QCT trajectories would be required for an exhaustive coverage of state space. For diatom-diatom collisions, which are relevant too in hypersonics, the number of transitions increases to $\sim 10^{15}$.[159] Clearly, it is neither possible nor meaningful to approach this problem using direct QCT simulations and alternative methods are required. One possibility consists of developing more coarse-grained models either by averaging over rotational energies, or by using energy-binning strategies,[160] to reduce the number of simulated transitions. However, it has been found that depending on the way how this coarse-graining is carried out, the internal energy distributions, relaxations and dissociation rates can be markedly different.[161,162] As an alternative, the direct molecular simulation (DMS) method has been developed.[163,164]

One recently explored possibility that can be applied to reactive and non-reactive state-to-state cross sections is to train a machine learned model based on neural networks from

explicit QCT data for state-to-state cross sections from which all necessary information can be determined.[165] Such an approach combines the accuracy of QCT simulations based on state-of-the art electronic structure calculations and PES representation techniques with the necessary speed to obtain the molecular-level data for nonreactive and reactive atom+diatom collisions. For this, the $N(^4S)+NO(X^2\Pi)(v,j) \rightarrow O(^3P)+N_2(X^1\Sigma_g^+)(v',j')$ reaction has been considered to model the state-to-cross sections on $^3A'$ PES. There are 6329 ro-vibrational states for the N+NO channel, and 8733 states for the O+N_2 channel giving rise to $\sim 10^7$ state-to-state transitions.

Using exhaustive QCT simulations on a subset of the total state space a NN was trained based on the ResNet architecture.[166,167] Importance sampling of impact parameter in the QCT simulations and averaging the neighbour states contributions to the cross sections drastically reduces the number of trajectories required for converge results. Two different NN model were constructed (i) based on state-to-state cross sections and (ii) based on total cross sections. The validity of the NN was established by predicting observables obtained from the NN and explicitly calculating them using QCT simulations. The NN model successfully captures the trends as well as the magnitudes of the rates from QCT. For most cases the relative errors are $< 5\%$ although for individual states they can differ by up to 17 %. Total rates $k(T)$ calculated from QCT simulations and predicted by the NN models agree to within a few percent. As another test, the distribution of the final vibrational and rotational states and the rovibrational energies of N_2 after N+NO collisions at different temperatures was calculated from QCT and compared with those from the NN. The NN correctly captures the shape of all distributions but lacks oscillatory features, in particular for the rotational distribution (see Figure 5). It was hence found that the NN provides a physically robust model based on validated, microscopic data from which information about nonequilibrium systems can be obtained, obviating the construction of models based on simple, empirical expressions.[168] As the evaluation time of the NN is on the order of seconds for 10^6 state-

to-state cross sections, this technique is suitable for direct use in DSMC simulations . The average error from the NN compared with the reference QCT data is ~ 5 %. This compares with errors ranging from 25 % to 60 % for vibrational relaxation rates and state-specific dissociation rates from a maximum entropy model for O_2 + O.[169]
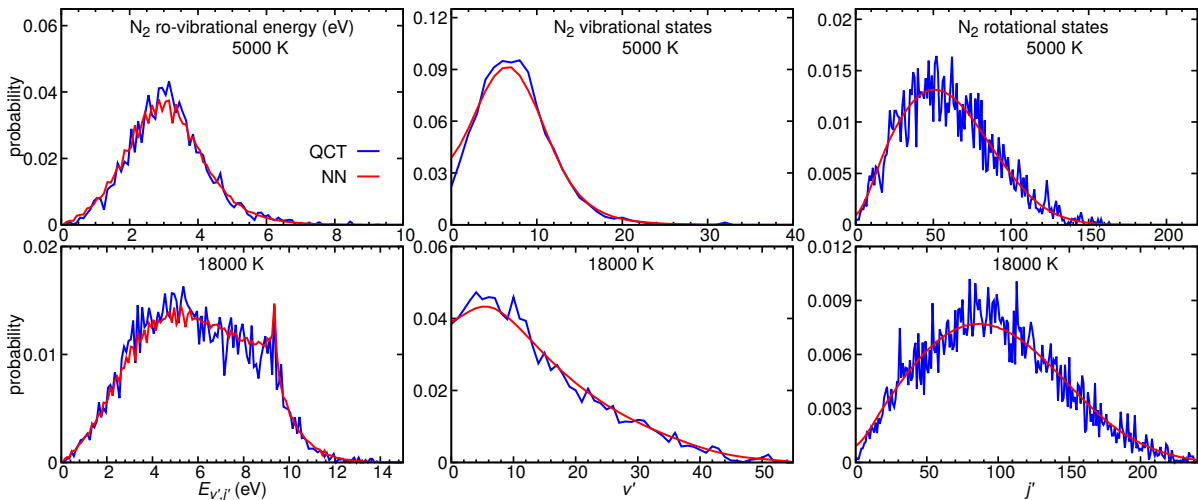

Figure 5: Distributions of product ro-vibrational states and ro-vibrational energies at 5000 and 18000 K for the N + NO $\rightarrow$ O + N_2 reaction calculated from QCT on the $^3A'$ PES (blue) and predicted by the NN state-to-state model (red), respectively. Data taken from Ref.[165]

Computing and learning the state-to-state cross sections for bi-molecular collisions is a tedious task as the number of possible transitions increases rapidly. For diatom-diatom collision systems the problem becomes intractable.[164] One possibility to avoid this is to train distributional models based on initial and final states and energy distributions at different ro-vibrational and translational temperatures using machine learning, similar to the model for state-to-state cross sections discussed above.

Hence from combining expertise and computational strategies rooted in different disciplines across chemical physics and computational chemistry it is expected that realistic, robust and computational tractable models based on accurate molecular processes can be built for reactive, rarefied flows at different thermodynamic conditions, including the hypersonic regime.

Such a model still requires approximations to be made. However, by using the highest possible level of theory at each step it is also expected that meaningful and informative error estimates can be provided as to the reliability of the models. One example is the question how sensitive the results of the QCT (or also quantum dynamics) simulations are to the local and global shape and quality of the PESs. Such sensitivity analyses can be computationally demanding in itself but become possible with the increased computational resources available.

Conclusions

As the field of reactive A+BC collisions continues to mature, quantitative assessment of the reliability and predictability of the underlying PESs and the type (quantum vs. classical) of dynamics become important in particular if the results are used in reaction networks or more coarse grained simulations. Every element in the chain from electronic structure calculations, coverage of conformational space, representation/fitting of the points, QCT/quantum simulations, and determining cross sections/rates from them has its own errors associated with it. Hence, when using rates or cross sections as input to more coarse grained treatments of reaction networks it is highly desirable to have realistic error estimates of the individual steps. This also provides the basis for targeted improvements of the data and input on which the more coarse grained simulations are based.

If sufficient high-quality experimental data is available, one promising tool that has been tested for high-resolution spectroscopy is the "morphing potential" approach.[170,171] It directly relates the PES with the observables and obviates all intermediate steps. However, to the best of our knowledge, this has never been attempted for reaction or vibrational relaxation rates.

In conclusion, describing reaction and vibrational relaxation rates and state-to-state cross sections relevant to hypersonics is a formidable problem extending over multiple length and time scales. The field requires cutting-edge expertise ranging from quantum chemistry and quantum/classical dynamics to chemical and mechanical engineering. The material discussed here demonstrates that atomistic simulations provide the necessary quantitative insight into nonequilibrium distributions for the different degrees of freedom, i.e. for $T_{\text{trans}} \neq T_{\text{rot}} \neq T_{\text{vib}}$, that are required for rarefied flow and flow on small length scales relevant in hypersonics.[158] Obtaining such information, the best methods affordable for the electronic structure calculations, their representation, running the molecular dynamics and analyzing them are required. With such tools in hand, progress can be made in this challenging and multifaceted field of molecular-level physico-chemical relevance and to connect it with the macroscopic world.

Additional Information

The postdoctoral fellow working on this project was Dr. D. Koner.

Publications from this grant are References 21,48,105,137,165,172–176.

Acknowledgement

References

(1) Desai, P. N.; Qualls, G. D. Stardust Entry Reconstruction. *J. Spacecraft Rock.* **2010**, *47*, 736–740.

(2) Boyd, I. Computation of atmospheric entry flow about a Leonid meteoroid. *Earth Moon Plan.* **1998**, *82-3*, 93–108.

(3) Anderson, J. D. *Hypersonic and High Temperature Gas Dynamics*; AIAA, 2006.

(4) Bertin, J.; Cummings, R. Fifty years of hypersonics: where we've been, where we're going. *Prog. Aerospace Sci.* **2003**, *39*, 511–536.

(5) Park, C. Review of Chemical-Kinetic Problems of Future NASA Missions. 1. Earth Entries. *J. Thermophys. Heat Transf.* **1993**, *7*, 385–398.

(6) Park, C.; Jaffe, R.; Partridge, H. Chemical-kinetic parameters of hyperbolic Earth entry. *J. Thermophys. Heat Transf.* **2001**, *15*, 76–90.

(7) Millikan, R. C.; White, D. R. Systematics of Vibrational Relaxation. *J. Chem. Phys.* **1963**, *39*, 3209–3213.

(8) Park, C.; Howe, J. T.; Jaffe, R. L.; Candler, G. V. Review of chemical-kinetic problems of future NASA missions. II-Mars entries. *J. Thermophys. Heat Transf.* **1994**, *8*, 9–23.

(9) Valentini, P.; Schwartzentruber, T. E.; Bender, J. D.; Candler, G. V. Dynamics of nitrogen dissociation from direct molecular simulation. *Phys. Rev. Fluids* **2016**, *1*.

(10) Panesi, M.; Jaffe, R. L.; Schwenke, D. W.; Magin, T. E. Rovibrational internal energy transfer and dissociation of $N_2(^1\Sigma_g^+)$-$N(^4S_u)$ system in hypersonic flows. *J. Chem. Phys.* **2013**, *138*, 044312.

(11) Denis-Alpizar, O.; Bemish, R. J.; Meuwly, M. Communication: Vibrational relaxation of CO($^1\Sigma$) in collision with Ar(^{1}S) at temperatures relevant to the hypersonic flight regime. *J. Chem. Phys.* **2017**, *146*, 111102.

(12) Bird, G. A. *Molecular Gas Dynamics and the Direct Simulation of Gas Flows*; Clarendon Press, 1994.

(13) Boyd, I.; Bose, D.; Candler, G. Monte Carlo modeling of nitric oxide formation based on quasi-classical trajectory calculations. *Phys. Fluids* **1997**, *9*, 1162–1170.

(14) Werner, H.; Knowles, P. J. A second order multiconfiguration SCF procedure with optimum convergence. *J. Chem. Phys.* **1985**, *82*, 5053–5063.

(15) Knowles, P. J.; Werner, H.-J. An efficient second-order MC SCF method for long configuration expansions. *Chem. Phys. Lett.* **1985**, *115*, 259 – 267.

(16) Werner, H.; Meyer, W. A quadratically convergent multiconfiguration-self-consistent field method with simultaneous optimization of orbitals and CI coefficients. *J. Chem. Phys.* **1980**, *73*, 2342–2356.

(17) Langhoff, S. R.; Davidson, E. R. Configuration Interaction calculations on Nitrogen Molecule. *Int. J. Quant. Chem.* **1974**, *8*, 61–72.

(18) Werner, H.; Knowles, P. J. An efficient internally contracted multiconfiguration-reference configuration interaction method. *J. Chem. Phys.* **1988**, *89*, 5803–5814.

(19) Knowles, P. J.; Werner, H.-J. An efficient method for the evaluation of coupling coefficients in configuration interaction calculations. *Chem. Phys. Lett.* **1988**, *145*, 514 – 522.

(20) Dunning, T. H. J. Gaussian basis sets for use in correlated molecular calculations. I. The atoms boron through neon and hydrogen. *J. Chem. Phys.* **1989**, *90*, 1007.

(21) Koner, D.; San Vicente Veliz, J. C.; van der Avoird, A.; Meuwly, M. Near dissociation states for H_2^+–He on MRCI and FCI potential energy surfaces. *Phys. Chem. Chem. Phys.* **2019**, *21*, 24976–24983.

(22) Franke, R.; Nielson, G. Smooth Interpolation of Large Sets of Scattered Data. *Int. J. Numer. Meth. Eng.* **1980**, *15*, 1691–1704.

(23) Nguyen, K. A.; Rossi, I.; Truhlar, D. G. A Dual-Level Shepard Interpolation Method for Generating Potential Energy Surfaces for Dynamics Calculations. *J. Chem. Phys.* **1995**, *103*, 5522–5530.

(24) Bettens, R. P.; Collins, M. A. Learning to Interpolate Molecular Potential Energy Surfaces with Confidence: A Bayesian Approach. *J. Chem. Phys.* **1999**, *111*, 816–826.

(25) Lancaster, P.; Salkauskas, K. Surfaces Generated by Moving Least Squares Methods. *Math. Comp.* **1981**, *37*, 141–158.

(26) Ischtwan, J.; Collins, M. A. Molecular Potential Energy Surfaces by Interpolation. *J. Chem. Phys.* **1994**, *100*, 8080–8088.

(27) Dawes, R.; Thompson, D. L.; Wagner, A. F.; Minkoff, M. Interpolating Moving Least-Squares Methods for Fitting Potential Energy Surfaces: A Strategy for Efficient Automatic Data Point Placement in High Dimensions. *J. Chem. Phys.* **2008**, *128*, 084107.

(28) Cassam-Chenaï, P.; Patras, F. Symmetry-Adapted Polynomial Basis for Global Potential Energy Surfaces-Applications to XY_4 Molecules. *J. Math. Chem.* **2008**, *44*, 938–966.

(29) Braams, B. J.; Bowman, J. M. Permutationally Invariant Potential Energy Surfaces in High Dimensionality. *Int. Rev. Phys. Chem.* **2009**, *28*, 577–606.

(30) Paukku, Y.; Yang, K. R.; Varga, Z.; Truhlar, D. G. Global Ab Initio Ground-State Potential Energy Surface of N_4. *J. Chem. Phys.* **2013**, *139*, 044309.

(31) Sumpter, B. G.; Noid, D. W. Potential Energy Surfaces for Macromolecules. A Neural Network Technique. *Chem. Phys. Lett.* **1992**, *192*, 455–462.

(32) Bowman, J. M.; Braams, B. J.; Carter, S.; Chen, C.; Czako, G.; Fu, B.; Huang, X.; Kamarchik, E.; Sharma, A. R.; Shepler, B. C.; *et al.*, Ab-Initio-Based Potential Energy Surfaces for Complex Molecules and Molecular Complexes. *J. Phys. Chem. Lett.* **2010**, *1*, 1866–1874.

(33) Jiang, B.; Li, J.; Guo, H. Potential Energy Surfaces from High Fidelity Fitting of Ab Initio Points: the Permutation Invariant Polynomial-Neural Network Approach. *Int. Rev. Phys. Chem.* **2016**, *35*, 479–506.

(34) Jordan, M. J.; Thompson, K. C.; Collins, M. A. The Utility of Higher Order Derivatives in Constructing Molecular Potential Energy Surfaces by Interpolation. *J. Chem. Phys.* **1995**, *103*, 9669–9675.

(35) Jordan, M. J.; Thompson, K. C.; Collins, M. A. Convergence of Molecular Potential Energy Surfaces by Interpolation: Application to the OH + $H_2 \rightarrow H_2O$ + H Reaction. *J. Chem. Phys.* **1995**, *102*, 5647–5657.

(36) Skokov, S.; Peterson, K. A.; Bowman, J. M. An Accurate Ab Initio HOCl Potential Energy Surface, Vibrational and Rotational Calculations, and Comparison with Experiment. *J. Chem. Phys.* **1998**, *109*, 2662–2671.

(37) Collins, M. A. Molecular Potential-Energy Surfaces for Chemical Reaction Dynamics. *Theor. Chem. Acc.* **2002**, *108*, 313–324.

(38) Duchovic, R. J.; Volobuev, Y. L.; Lynch, G. C.; Truhlar, D. G.; Allison, T. C.; Wagner, A. F.; Garrett, B. C.; Corchado, J. C. POTLIB 2001: A Potential Energy Surface Library for Chemical Systems. *Comput. Phys. Commun.* **2002**, *144*, 169–187.

(39) Zhang, X.; Braams, B. J.; Bowman, J. M. An Ab Initio Potential Surface Describing Abstraction and Exchange for H + CH$_4$. *J. Chem. Phys.* **2006**, *124*, 021104.

(40) Li, J.; Wang, Y.; Jiang, B.; Ma, J.; Dawes, R.; Xie, D.; Bowman, J. M.; Guo, H. Communication: A Chemically Accurate Global Potential Energy Surface for the HO + CO → H + CO$_2$ Reaction. *J. Chem. Phys.* **2012**, *136*, 041103.

(41) Ho, T.-S.; Rabitz, H. A General Method for Constructing Multidimensional Molecular Potential Energy Surfaces from Ab Initio Calculations. *J. Chem. Phys.* **1996**, *104*, 2584–2597.

(42) Hollebeek, T.; Ho, T.-S.; Rabitz, H. A Fast Algorithm for Evaluating Multidimensional Potential Energy Surfaces. *J. Chem. Phys.* **1997**, *106*, 7223–7227.

(43) Hollebeek, T.; Ho, T.-S.; Rabitz, H. Constructing Multidimensional Molecular Potential Energy Surfaces from Ab Initio Data. *Annu. Rev. Phys. Chem.* **1999**, *50*, 537–570.

(44) Unke, O. T.; Meuwly, M. Toolkit for the Construction of Reproducing Kernel-Based Representations of Data: Application to Multidimensional Potential Energy Surfaces. *J. Chem. Inf. Model.* **2017**, *57*, 1923–1931.

(45) Rupp, M. Machine Learning for Quantum Mechanics in a Nutshell. *Int. J. Quantum Chem.* **2015**, *115*, 1058–1073.

(46) Aronszajn, N. Theory of Reproducing Kernels. *Trans. Amer. Math. Soc.* **1950**, *68*, 337–404.

(47) Hofmann, T.; Schölkopf, B.; Smola, A. J. Kernel methods in machine learning. *Ann. Stat.* **2008**, 1171–1220.

(48) Koner, D.; Bemish, R. J.; Meuwly, M. The C(^{3}P) + NO(X^{2}Π) → O(^{3}P) + CN(X^{2}Σ$^+$), N(^{2}D)/N(^{4}S) + CO(X^{1}Σ$^+$) reaction: Rates, branching ratios, and final states from 15 K to 20 000 K. *J. Chem. Phys.* **2018**, *149*, 094305.

(49) Unke, O. T.; Castro-Palacio, J. C.; Bemish, R. J.; Meuwly, M. Collision-Induced Rotational Excitation in N_2^+ ($^2\Sigma_g^+$, $\nu = 0$)–Ar: Comparison of Computations and Experiment. *J. Chem. Phys.* **2016**, *144*, 224307.

(50) Ho, T.-S.; Hollebeek, T.; Rabitz, H.; Harding, L. B.; Schatz, G. C. A Global H_2O Potential Energy Surface for the Reaction $O(^1D) + H_2 \rightarrow OH + H$. *J. Chem. Phys.* **1996**, *105*, 10472–10486.

(51) Meuwly, M.; Hutson, J. The potential energy surface and near-dissociation states of He-H_2^+. *J. Chem. Phys.* **1999**, *110*, 3418–3427.

(52) Dhont, G.; van Lenthe, J.; Groenenboom, G.; van der Avoird, A. Ab initio calculation of the $NH(^3\Sigma^-)$-$NH(^3\Sigma^-)$ interaction potentials in the quintet, triplet, and singlet states. *J. Chem. Phys.* **2005**, *123*.

(53) van der Avoird, A.; Pedersen, T. B.; Dhont, G. S. F.; Fernandez, B.; Koch, H. Ab initio potential-energy surface and rovibrational states of the HCN-HCl complex. *J. Chem. Phys.* **2006**, *124*.

(54) Schölkopf, B.; Herbrich, R.; Smola, A. J. A Generalized Representer Theorem. International Conference on Computational Learning Theory. 2001; pp 416–426.

(55) Golub, G. H.; Van Loan, C. F. *Matrix Computations*; JHU Press Baltimore, 2012; Vol. 3.

(56) Vargas-Hernandez, R. A.; Guan, Y.; Zhang, D. H.; Krems, R., V Bayesian optimization for the inverse scattering problem in quantum reaction dynamics. *New J. Phys.* **2019**, *21*, 022001.

(57) Qu, C.; Bowman, J. M. A fragmented, permutationally invariant polynomial approach for potential energy surfaces of large molecules: Application to N-methyl acetamide. *J. Chem. Phys.* **2019**, *150*.

(58) Troe, J. The Dependence of Unimolecular Reaction-Rates on the Anisotropy of Potential-Energy Surfaces. *Z. Phys. Chem. Neue Folge* **1989**, *161*, 209–232.

(59) Harding, L.; Stark, H.; Troe, J.; Ushakov, V. New studies of the unimolecular reaction NO_2 reversible arrow O+NO. Part 2. Relation between high pressure rate constants and potential parameters. *Phys. Chem. Chem. Phys.* **1999**, *1*, 63–72.

(60) Hutson, J. M. Intermolecular Forces from the Spectroscopy of Vanderwaals Molecules. *Annu. Rev. Phys. Chem.* **1990**, *41*, 123–154.

(61) Nagy, T.; Yosa Reyes, J.; Meuwly, M. Multisurface Adiabatic Reactive Molecular Dynamics. *J. Chem. Theor. Comp.* **2014**, *10*, 1366–1375.

(62) Truhlar, D. G.; Muckerman, J. T. In *Atom - Molecule Collision Theory*; Bernstein, R. B., Ed.; Springer US, 1979; pp 505–566.

(63) Koner, D. *Scattering studies of proton transfer reactions between rare gas atoms*; Indian Institute of Technology Guwahati, 2016.

(64) Althorpe, S.; Clary, D. Quantum scattering calculations on chemical reactions. *Annu. Rev. Phys. Chem.* **2003**, *54*, 493–529.

(65) Bonnet, L.; Rayez, J.-C. Quasiclassical Trajectory Method for Molecular Scattering Processes: Necessity of a Weighted Binning Approach. *Chem. Phys. Lett.* **1997**, *277*, 183–190.

(66) Bonnet, L.; Rayez, J.-C. Gaussian Weighting in the Quasiclassical Trajectory Method. *Chem. Phys. Lett.* **2004**, *397*, 106–109.

(67) Koner, D.; Barrios, T., Lizandra andGonzález-Lezana; Panda, A. N. State-to-State Dynamics of the Ne + $HeH^+(v = 0, j = 0) \rightarrow NeH^+(v', j')$ + He Reaction. *J. Phys. Chem. A* **2016**, *120*, 4731–4741.

(68) Billing, G. D. Classical Path Method in Inelastic and Reactive Scattering. *Int. Rev. Phys. Chem.* **1994**, *13*, 309–335.

(69) Tully, J. Molecular Dynamics with Electronic Transitions. *J. Chem. Phys.* **1990**, *93*, 1061–1071.

(70) McLachlan, A. D. A variational solution of the time-dependent Schrodinger equation. *Mol. Phys.* **1964**, *8*, 39–44.

(71) Stine, J. R.; Muckerman, J. T. On the multidimensional surface intersection problem and classical trajectory "surface hopping". *J. Chem. Phys.* **1976**, *65*, 3975.

(72) Landau, L. D. Zur Theorie der Energieubertragung. II. *Phys. Z* **1932**, *2*, 46–51.

(73) Zener, C. Non-adiabatic crossing of energy levels. *Proc. R. Soc. London A* **1932**, *137*, 696–702.

(74) Belyaev, A. K.; Lebedev, O. V. . *Phys. Rev. A* **2011**, *84*, 014701.

(75) Belyaev, A. K.; Lasser, C.; Trigila, G. Landau-Zener type surface hopping algorithms. *J. Chem. Phys.* **2014**, *140*.

(76) Miller, W. H.; George, T. F. Semiclassical Theory of Electronic Transitions in Low Energy Atomic and Molecular Collisions Involving Several Nuclear Degrees of Freedom. *J. Chem. Phys.* **1972**, *56*, 5637.

(77) Nyman, G.; Yu, H. Quantum theory of bimolecular chemical reactions. *Rep. Prog. Phys.* **2000**, *63*, 1001–1059.

(78) Hutson, J. M.; Le Sueur, C. R. MOLSCAT: A program for non-reactive quantum scattering calculations on atomic and molecular collisions. *Comput. Phys. Commun.* **2019**, *241*, 9–18.

(79) Peng, T.; Zhang, D.; Wang, D.; Li, Y.; Zhang, J. Dynasol: A visual quantum dynamics package. *Comput. Phys. Commun.* **2000**, *128*, 492–495.

(80) Skouteris, D.; Castillo, J.; Manolopoulos, D. ABC: a quantum reactive scattering program. *Comput. Phys. Commun.* **2000**, *133*, 128–135.

(81) Kosloff, R. Time-dependent quantum-mechanical methods for molecular dynamics. *J. Phys. Chem.* **1988**, *92*, 2087–2100.

(82) Tannor, D. J. *Introduction to quantum mechanics: A time dependent perspective*; University Science Books, 2006.

(83) Feit, M. D.; J. A. Fleck, J.; Steiger, A. Solution of the Schödinger Equation by a Spectral Method. *J. Comp. Phys.* **1982**, *47*, 412 – 433.

(84) Tal-Ezer, H.; Kosloff, R. An accurate and efficient scheme for propagating the time dependent Schrödinger equation. *J. Chem. Phys.* **1984**, *81*, 3967–3971.

(85) Chen, R.; Guo, H. Evolution of quantum system in order domain of Chebyshev operator. *J. Chem. Phys.* **1996**, *105*, 3569–3578.

(86) Gray, S. K.; Balint-Kurti, G. G. Quantum Dynamics with Real Wave Packets, Including Application to Three-Dimensional (J=0) $D+H_2 \rightarrow HD+H$ Reactive Scattering. *J. Chem. Phys.* **1998**, *108*, 950–962.

(87) Chen, R.; Guo, H. The Chebyshev propagator for quantum systems. *Comput. Phys. Commun.* **1999**, *119*, 19–31.

(88) Mandelshtam, V. A.; Taylor, H. S. Spectral Projection Approach to the Quantum Scattering Calculations. *J. Chem. Phys.* **1995**, *102*, 7390–7399.

(89) Manolopoulos, D. E. Derivation and reflection properties of a transmission-free absorbing potential. *J. Chem. Phys.* **2002**, *117*, 9552–9559.

(90) Panda, A. N.; Sathyamurthy, N. Time-Dependent Quantum Mechanical Wave Packet Study of the He + H_2^+ (v, j) $\rightarrow$ HeH^+ + H Reaction. *J. Chem. Phys.* **2005**, *122*, 054304.

(91) Defazio, P.; Petrongolo, C.; Oliva, C.; González, M.; Sayós, R. Quantum dynamics of the $N(^4S)+O_2$ reaction on the X^2A' and a^4A' surfaces: Reaction probabilities, cross sections, rate constants, and product distributions. *J. Chem. Phys.* **2002**, *117*, 3647–3655.

(92) Gamallo, P.; González, M.; Sayós, R.; Petrongolo, C. Quantum wave packet dynamics of the $1^3A''N(^4S)+NO(\tilde{X}^2\Pi)\rightarrow N_2(\tilde{X}^1\Sigma_g^+)+O(^3P)$ reaction. *J. Chem. Phys.* **2003**, *119*, 7156–7162.

(93) Miquel, I.; González, M.; Sayós, R.; Balint-Kurti, G. G.; Gray, S. K.; Goldfield, E. M. Quantum reactive scattering calculations of cross sections and rate constants for the $N(^2D) + O_2(X^3\Sigma_g^-) \rightarrow O(^3P) + NO(X\ ^2\Pi)$ reaction. *J. Chem. Phys.* **2003**, *118*, 3111–3123.

(94) Gamallo, P.; Sayos, R.; Gonzalez, M.; Petrongolo, C.; Defazio, P. Quantum real wave-packet dynamics of the $N(^4S)+ NO(\tilde{X}^2\Pi) \rightarrow N_2\ (\tilde{X}^1\Sigma_g^+)+ O(^3P)$ reaction on the ground and first excited triplet potential energy surfaces: Rate constants, cross sections, and product distributions. *J. Chem. Phys.* **2006**, *124*, 174303.

(95) Abrahamsson, E.; Andersson, S.; Markovic, N.; Nyman, G. Dynamics of the O + CN Reaction and N + CO Scattering on Two Coupled Surfaces. *J. Phys. Chem. A* **2009**, *113*, 14824–14830.

(96) Koner, D.; Barrios, L.; González-Lezana, T.; P anda, A. N. Scattering study of the Ne + $NeH^+(v_0 = 0, j_0 = 0) \rightarrow NeH^+$ + Ne reaction on an ab initio based analytical potential energy surface. *J. Chem. Phys.* **2016**, *144*, 034303.

(97) Zeldovich, Y. The Oxidation of Nitrogen in Combustion Explosions. *Acta Physicochimica U.S.S.R.* **1946**, *21*, 577–628.

(98) Bose, D.; Candler, G. V. Thermal rate constants of the $O_2 + N \rightarrow NO + O$ reaction based on the $^2A'$ and $^4A'$ potential-energy surfaces. *J. Chem. Phys.* **1997**, *107*, 6136–6145.

(99) Dodd, J. A.; Lockwood, R. B.; Hwang, E. S.; Miller, S. M.; Lipson, S. J. Vibrational relaxation of NO(v=1) by oxygen atoms. *J. Chem. Phys.* **1999**, *111*, 3498–3507.

(100) Gupta, R.; Yos, J.; Thompson, R.; Lee, K. A Review of Reaction Rates and Thermodynamic and Transport Properties for an 11-Species Air Model for Cheical and Thermal Nonequilibrium Calculations to 30000 K. *NASA Reference Publication 1232* **1990**,

(101) Sayós, R.; Oliva, C.; González, M. New analytical ($^2A'$, $^4A'$) surfaces and theoretical rate constants for the $N(^4S)+O_2$ reaction. *J. Chem. Phys.* **2002**, *117*, 670–679.

(102) Varandas, A. A realistic multi-sheeted potential energy surface for $NO_2(^2A')$ from the double many-body expansion method and a novel multiple energy-switching scheme. *J. Chem. Phys.* **2003**, *119*, 2596–2613.

(103) Mota, V. C.; Caridade, P. J. S. B.; Varandas, A. J. C. Ab Initio-Based Global Double Many-Body Expansion Potential Energy Surface for the First $^2A''$ Electronic State of NO_2. *J. Phys. Chem. A* **2012**, *116*, 3023–3034.

(104) Castro-Palacio, J. C.; Nagy, T.; Bemish, R. J.; Meuwly, M. Computational Study of Collisions Between $O(^3P)$ and $NO(^2\Pi)$ at Temperatures Relevant to the Hypersonic Flight Regime. *J. Chem. Phys.* **2014**, *141*, 164319.

(105) San Vicente Veliz, J. C.; Koner, D.; Schwilk, M.; Bemish, R. J.; Meuwly, M. The $N(^4S) + O_2(X^3\Sigma_g^-) \leftrightarrow O(^3P) + NO(X^2\Pi)$ Reaction: Thermal and Vibrational Re-

laxation Rates for the ^{2}A′, ^{4}A′ and ^{2}A″ States. *Phys. Chem. Chem. Phys.* **2020**, 10.1039/C9CP06085E.

(106) Fernandez, A.; Goumri, A.; Fontijn, A. Kinetics of the Reactions of N(^{4}S) Atoms with O$_2$ and CO$_2$ over Wide Temperatures Ranges. *J. Phys. Chem. A* **1998**, *102*, 168–172.

(107) Caridade, P. J. B. S.; Varandas, A. J. C. Dynamics Study of the N(^{4}S) + O$_2$ Reaction and Its Reverse. *J. Phys. Chem. A* **2004**, *108*, 3556–3564.

(108) Livesey, J. B.; Roberts, A. L.; Williams, A. The Formation of Oxides of Nitrogen in some Oxy-Propane Flames. *Combust. Sci. Technol.* **1971**, *4*, 9–15.

(109) Kaufman, F.; Decker, L. Effect of oxygen on thermal decomposition of nitric oxide at high temperatures. *7th Symp (Int.) on Combustion* **1958**, *7*, 57 – 60.

(110) Kolsbjerg, E. L.; Groves, M. N.; Hammer, B. An automated nudged elastic band method. *J. Chem. Phys.* **2016**, *145*, 094107.

(111) Castro-Palacio, J. C.; Bemish, R. J.; Meuwly, M. Communication: Equilibrium rate coefficients from atomistic simulations: The O(^{3}P) + NO(^{2}Π) → O$_2$ (X$^3\Sigma_g^-$) + N(^{4}S) reaction at temperatures relevant to the hypersonic flight regime. *J. Chem. Phys.* **2015**, *142*, 091104.

(112) Gordon,; McBride, J. *Computer program for calculation of complex chemical equilibrium compositions and applications. I: Analysis*; NASA Reference publication, 1996; Vol. 19; p 1311.

(113) Hwang, E. S.; Castle, K. J.; Dodd, J. A. Vibrational relaxation of NO(v = 1) by oxygen atoms between 295 and 825 K. *J. Geophys. Res.* **2003**, *108*, 1109.

(114) Fernando, R. P.; Smith, I. W. Vibrational relaxations of NO by atomic oxygen. *Chem. Phys. Lett.* **1979**, *66*, 218 – 222.

(115) Ivanov, M. V.; Schinke, R.; Mcbane, G. C. Theoretical investigation of vibrational relaxation of NO($^2\Pi$), O$_2$($^3\Sigma_g^-$), and N$_2$($^1\Sigma_g^+$) in collisions with O(^{3}P). *Mol. Phys.* **2007**, *105*, 1183–1191.

(116) Caridade, P. J. S. B.; Li, J.; Mota, V. C.; Varandas, A. J. C. The O + NO(v) Vibrational Relaxation Processes Revisited. *J. Phys. Chem. A* **2018**, *122*, 5299–5310.

(117) Anderson, S. M.; Klein, F. S.; Kaufman, F. Kinetics of the isotope exchange reaction of 18O with NO and O2 at 298 K. *J. Chem. Phys.* **1985**, *83*, 1648–1656.

(118) Lilenfeld, H. V. Deactivation of vibrationally excited NO and CO$_2$ by OâĂŘatoms. *Phillips Laboratory, Hanscom Air Force Base, Mass* **1994**, *PL-TR-94-2180*, 24pp.

(119) Glänzer, K.; Troe, J. Vibrational relaxation of NO in collisions with atomic oxygen and chlorine. *J. Chem. Phys.* **1975**, *63*, 4352–4357.

(120) Caridade, P. J. S. B.; Mota, V. C.; Mohallem, J. R.; Varandas, A. J. C. A Theoretical Study of Rate Coefficients for the O + NO Vibrational Relaxation. *J. Phys. Chem. A* **2008**, *112*, 960–965.

(121) Gamallo, P.; González, M.; Sayós, R. Ab initio derived analytical fits of the two lowest triplet potential energy surfaces and theoretical rate constants for the N(^{4}S)+ NO(X$^2\Pi$) system. *J. Chem. Phys.* **2003**, *119*, 2545–2556.

(122) Lin, W.; Varga, Z.; Song, G.; Paukku, Y.; Truhlar, D. G. Global triplet potential energy surfaces for the N$_2$(X$^1\Sigma$)+O(^3P) $\rightarrow$ NO($X^2\Pi$) + N(^4S) reaction. *J. Chem. Phys.* **2016**, *144*, 024309.

(123) Denis-Alpizar, O.; Bemish, R. J.; Meuwly, M. Reactive collisions for NO($^2\Pi$) + N(^{4}S) at temperatures relevant to the hypersonic flight regime. *Phys. Chem. Chem. Phys.* **2017**, *19*, 2392.

(124) Lee, J.; Michael, J.; Payne, W.; Stief, L. Absolute rate of the reaction of N(^{4}S) with NO from 196-400 K with DF–RF and FP–RF techniques. *J. Chem. Phys.* **1978**, *69*, 3069–3076.

(125) Michael, J. V.; Lim, K. P. Rate constants for the N_2O reaction system: Thermal decomposition of N_2O; N+NO $\rightarrow$ N_2+O; and implications for O+N_2 $\rightarrow$ NO+N. *J. Chem. Phys.* **1992**, *97*, 3228–3234.

(126) Mick, H. J.; Matsui, H.; Roth, P. High-temperature kinetics of silicon atom oxidation by nitric oxide based on silicon, nitrogen, and oxygen atom measurements. *J. Phys. Chem.* **1993**, *97*, 6839–6842.

(127) Bergeat, A.; Hickson, K. M.; Daugey, N.; Caubet, P.; Costes, M. A low temperature investigation of the N(^{4}S) + NO reaction. *Phys. Chem. Chem. Phys.* **2009**, *11*, 8149–8155.

(128) Monat, J.; Hanson, R.; Kruger, C. Shock tube determination of the rate coefficient for the reaction N_2+O $\rightarrow$ NO+N. Symposium (International) on Combustion. 1979; pp 543–552.

(129) Thielen, K.; Roth, P. Resonance absorption measurements of N and O atoms in high temperature NO dissociation and formation kinetics. Symposium (International) on Combustion. 1985; pp 685–693.

(130) Gamallo, P.; Martínez, R.; Sayós, R.; González, M. Quasiclassical dynamics and kinetics of the N + NO $\rightarrow$ N_2 + O, NO + N atmospheric reactions. *J. Chem. Phys.* **2010**, *132*, 144304.

(131) Bose, D.; Candler, G. V. Thermal rate constants of the N_2+O$\rightarrow$NO+N reaction using ab initio ^{3}A″ and ^{3}A′ potential energy surfaces. *J. Chem. Phys.* **1996**, *104*, 2825–2833.

(132) Thielen, K.; Roth, P. Resonance absorption measurements of N and O atoms in high temperature no dissociation and formation kinetics. *Symp. (Int.) Combust.* **1985**, *20*, 685 – 693.

(133) Baulch, D. L.; Bowman, C. T.; Cobos, C. J.; Cox, R. A.; Just, T.; Kerr, J. A.; Pilling, M. J.; Stocker, D.; Troe, J.; Tsang, W.; Walker, R. W.; Warnatz, J. Evaluated Kinetic Data for Combustion Modeling: Supplement II. *J. Phys. Chem. Ref. Data* **2005**, *34*, 757–1397.

(134) Wennberg, P. O.; Anderson, J. G.; Weisenstein, D. K. Kinetics of reactions of ground state nitrogen atoms (^{4}S$_{3/2}$) with NO and NO$_2$. *J. Geophys. Res. Atmos.* **1994**, *99*, 18839–18846.

(135) Luo, H.; Kulakhmetov, M.; Alexeenko, A. Ab initio state-specific N$_2$ + O dissociation and exchange modeling for molecular simulations. *J. Chem. Phys.* **2017**, *146*, 074303.

(136) Esposito, F.; Armenise, I. Reactive, Inelastic, and Dissociation Processes in Collisions of Atomic Oxygen with Molecular Nitrogen. *J. Phys. Chem. A* **2017**, *121*, 6211–6219.

(137) Koner, D.; Veliz, J. C. S. V.; Bemish, R. J.; Meuwly, M. Accurate Reproducing Kernel-Based Potential Energy Surfaces for the Triplet Ground States of N$_2$O and Dynamics for the N+NO↔O+N$_2$ Reaction. *Phys. Chem. Chem. Phys.* **2020**, *22*, 18488–18498.

(138) Breshears, W. D.; Bird, P. F. Effect of Oxygen Atoms on the Vibrational Relaxation of Nitrogen. *J. Chem. Phys.* **1968**, *48*, 4768–4773.

(139) McNeal, R.; Whitson, M.; Cook, G. Quenching of vibrationally excited N$_2$ by atomic oxygen. *Chem. Phys. Lett.* **1972**, *16*, 507–510.

(140) Eckstrom, D. J. Vibrational relaxation of shock-heated N$_2$ by atomic oxygen using the IR tracer method. *J. Chem. Phys.* **1973**, *59*, 2787–2795.

(141) Bethe, H. A.; Teller, E. *Deviations from Thermal Equilibrium in Shock Waves*; Ballistic Research Labs, 1941; Vol. X-117.

(142) Capitelli, M.; Ferreira, C. M.; Gordiets, B. F.; Osipov, A. I. *Plasma Kinetics in Atmospheric Gases*; Springer-Verlag Berlin Heidelberg, 2000.

(143) Lamoureux, N.; El Merhubi, H.; Pillier, L.; de Persis, S.; Desgroux, P. Modeling of NO formation in low pressure premixed flames. *Comb. Flame* **2016**, *163*, 557–575.

(144) Johnston, C. O.; Brandis, A. M. Modeling of nonequilibrium CO Fourth-Positive and CN Violet emission in CO_2-N_2 gases. *J. Quant. Spectrosc. Radiat. Transfer* **2014**, *149*, 303–317.

(145) Husain, D.; Kirsch, L. J. Kinetic investigation of $C(2^3P_J)$ by photoelectric measurement of the attenuation of atomic emission in the vacuum ultra-violet. *Chem. Phys. Lett.* **1971**, *8*, 543–546.

(146) Husain, D.; Young, A. N. Kinetic investigation of ground state carbon atoms, $C(2^3P_J)$. *J. Chem. Soc., Faraday Trans. 2* **1975**, *71*, 525–531.

(147) Dean, A. J.; Hanson, R. K.; Bowman, C. T. A shock tube study of reactions of carbon atoms and methylidyne with nitric oxide including product channel measurements. *J. Phys. Chem.* **1991**, *95*, 3180.

(148) Chastaing, D.; Le Picard, S. D.; Sims, I. R. Direct kinetic measurements on reactions of atomic carbon, $C(^3P)$, with O_2 and NO at temperatures down to 15 K. *J. Chem. Phys.* **2000**, *112*, 8466.

(149) Simonson, M.; Marković, N.; Nordholm, S.; Persson, B. J. Quasiclassical trajectory study of the C + NO reaction on a new potential energy surface. *Chem. Phys.* **1995**, *200*, 141–160.

(150) Andersson, S.; Marković, N.; Nyman, G. An improved potential energy surface for the C + NO reaction. *Phys. Chem. Chem. Phys.* **2000**, *2*, 613–620.

(151) Andersson, S.; Marković, N.; Nyman, G. Quasi-classical trajectory simulations of C + NO crossed molecular beam experiments. *Chem. Phys.* **2000**, *259*, 99–108.

(152) Abrahamsson, E.; Andersson, S.; Marković, N.; Nyman, G. An improved potential energy surface for the C + NO reaction. *Phys. Chem. Chem. Phys.* **2008**, *10*, 4400–4409.

(153) Andersson, S.; Marković, N.; Nyman, G. Computational Studies of the Kinetics of the C + NO and O + CN Reactions. *J. Phys. Chem. A* **2003**, *107*, 5439–5447.

(154) Frankcombe, T. J.; Andersson, S. An Adiabatic Capture Theory and Quasiclassical Trajectory Study of C + NO and O + CN on the $^2A'$, $^2A''$ and $^4A''$ Potential Energy Surfaces. *J. Phys. Chem. A* **2012**, *116*, 4705–4711.

(155) Gonçalves, C.; Galvão, B.; Mota, V.; Braga, J.; Varandas, A. Accurate explicit-correlation-MRCI-based DMBE potential-energy surface for ground-state CNO. *J. Phys. Chem. A* **2018**, *122*, 4198–4207.

(156) Alves, M. V.; Gonçalves, C. E. M.; Braga, J. P.; Mota, V. C.; Varandas, A. J. C.; Galvão, B. R. L. Quasiclassical Study of the C(^{3}P) + NO(X^{2}Π) and O(^{3}P) + CN(X^{2}Σ$^+$) Collisional Processes on an Accurate DMBE Potential Energy Surface. *J. Phys. Chem. A* **2019**, *123*, 7195–7200.

(157) Pezzella, M.; Koner, D.; Meuwly, M. Formation and Stabilization of Ground and Excited-State Singlet O_2 upon Recombination of ^{3}P Oxygen on Amorphous Solid Water. *J. Phys. Chem. Lett.* **2020**, *11*, 2171–2176.

(158) Boyd, I. D. Computation of Hypersonic Flows Using the Direct Simulation Monte Carlo Method. *J. Spacecraft Rock.* **2015**, *52*, 38–53.

(159) Grover, M. S.; Torres, E.; Schwartzentruber, T. E. Direct molecular simulation of internal energy relaxation and dissociation in oxygen. *Phys. Fluids* **2019**, *31*.

(160) Macdonald, R. L.; Jaffe, R. L.; Schwenke, D. W.; Panesi, M. Construction of a coarse-grain quasi-classical trajectory method. I. Theory and application to N_2-N_2 system. *J. Chem. Phys.* **2018**, *148*, 054309.

(161) Andrienko, D. A.; Boyd, I. D. Rovibrational energy transfer and dissociation in O_2-O collisions. *J. Chem. Phys.* **2016**, *144*, 104301.

(162) Torres, E.; Magin, T. E. Coupling of state-resolved rovibrational coarse-grain model for nitrogen to stochastic particle method for simulating internal energy excitation and dissociation. *J. Chem. Phys.* **2018**, *149*, 174106.

(163) Koura, K. Monte Carlo direct simulation of rotational relaxation of diatomic molecules using classical trajectory calculations: Nitrogen shock wave. *Phys. Fluids* **1997**, *9*, 3543–3549.

(164) Schwartzentruber, T. E.; Grover, M. S.; Valentini, P. Direct Molecular Simulation of Nonequilibrium Dilute Gases. *J. Thermophys. Heat Transf.* **2018**, *32*, 892–903.

(165) Koner, D.; Unke, O. T.; Boe, K.; Bemish, R. J.; Meuwly, M. Exhaustive state-to-state cross sections for reactive molecular collisions from importance sampling simulation and a neural network representation. *J. Chem. Phys.* **2019**, *150*, 211101.

(166) He, K.; Zhang, X.; Ren, S.; Sun, J. *Deep Residual Learning for Image Recognition. Proceedings of the IEEE Conference on Computer Vision and Pattern Recognition.* **2016**, 770–778.

(167) Unke, O. T.; Meuwly, M. PhysNet: A Neural Network for Predicting Energies, Forces, Dipole Moments, and Partial Charges. *J. Chem. Theor. Comp.* **2019**, *15*, 3678–3693.

(168) Singh, N.; Schwartzentruber, T. Nonequilibrium internal energy distributions during dissociation. *Proc. Natl. Acad. Sci.* **2018**, *115*, 47–52.

(169) Kulakhmetov, M.; Gallis, M.; Alexeenko, A. Ab initio-informed maximum entropy modeling of rovibrational relaxation and state-specific dissociation with application to the $O_2 + O$ system. *J. Chem. Phys.* **2016**, *144*, 174302.

(170) Meuwly, M.; Hutson, J. M. Morphing *ab initio* potentials: A systematic study of Ne–HF. *J. Chem. Phys.* **1999**, *110*, 8338–8347.

(171) Gazdy, B.; Bowman, J. An adjusted potential surface for HCN based on rigorous vibrational calculations. *J. Chem. Phys.* **1991**, *95*, 6309–6316.

(172) Koner, D.; Bemish, R. J.; Meuwly, M. Dynamics on multiple potential energy surfaces: Quantitative studies of elementary processes relevant to hypersonics. *J. Phys. Chem. A* **2020**, *124*, 6255–6269.

(173) Arnold, J.; Koner, D.; Käser, S.; Singh, N.; Bemish, R. J.; Meuwly, M. Machine Learning for Observables: Reactant to Product State Distributions for Atom–Diatom Collisions. *J. Phys. Chem. A* **2020**, *124*, 7177–7190.

(174) Koner, D.; Meuwly, M. Permutationally invariant, reproducing kernel-based potential energy surfaces for polyatomic molecules: From formaldehyde to acetone. *J. Chem. Theor. Comp.* **2020**, *16*, 5474–5484.

(175) Koner, D.; Salehi, S. M.; Mondal, P.; Meuwly, M. Non-conventional force fields for applications in spectroscopy and chemical reaction dynamics. *J. Chem. Phys.* **2020**, *153*, 010901.

(176) Veliz, J. C. S. V.; Koner, D.; Schwilk, M.; Bemish, R. J.; Meuwly, M. The $C(^3P)+ O_2$ $(^3\Sigma_g^-) \rightarrow CO_2 \leftrightarrow CO(^1\Sigma^+) + O(^1D)/O(^3P)$ reaction: thermal and vibrational

relaxation rates from 15 K to 20000 K. *Phys. Chem. Chem. Phys.* **2021**, *23*, 11251–11263.